Supporting Information

Synthesis, Structures and Magnetic Properties of Fe(II) and Co(II) Thiocyanato Coordination Compounds: On the Importance of the Diamagnetic Counterparts for Structure Determination.

Susanne Wöhlert, Lars Peters and Christian Näther

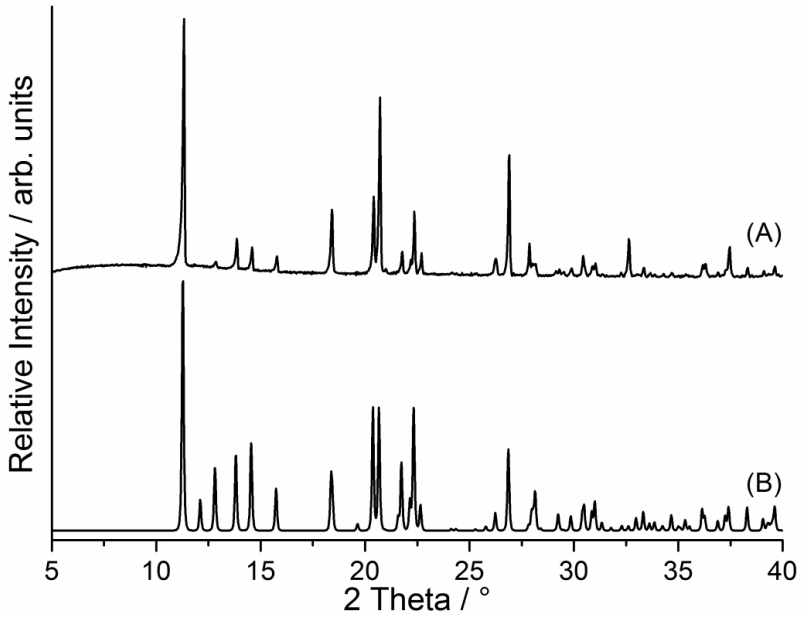

Fig. S1. Experimental XRPD pattern of **1-Co** (A) together with the powder pattern calculated from single crystal data (B).

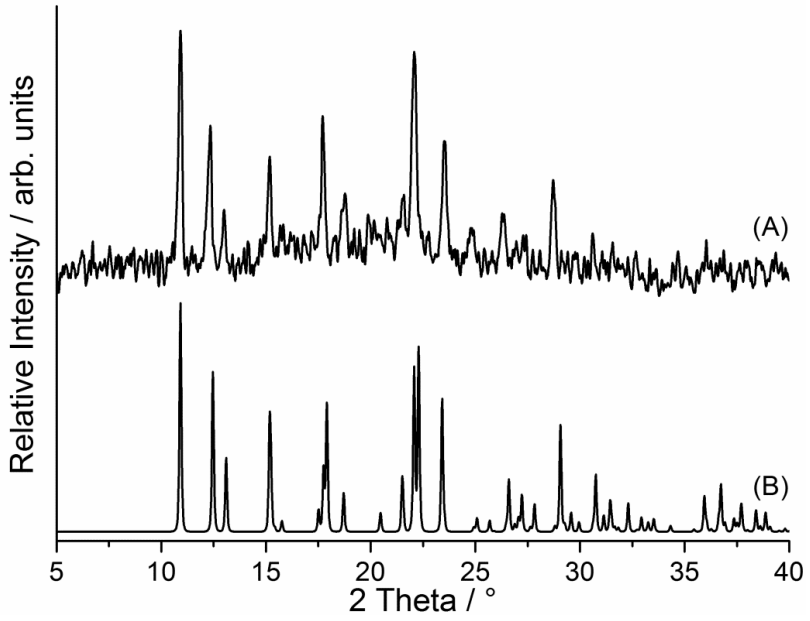

Fig. S2. Experimental XRPD pattern of **2-Co** (A) together with the powder pattern calculated from single crystal data (B).

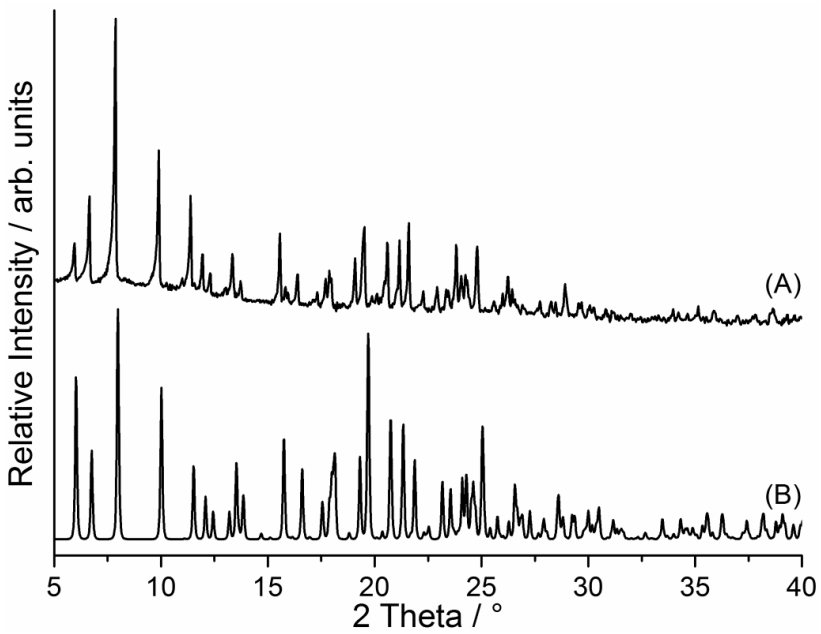

Fig. S3. Experimental XRPD pattern of **3-Co** (A) together with the powder pattern calculated from single crystal data (B).

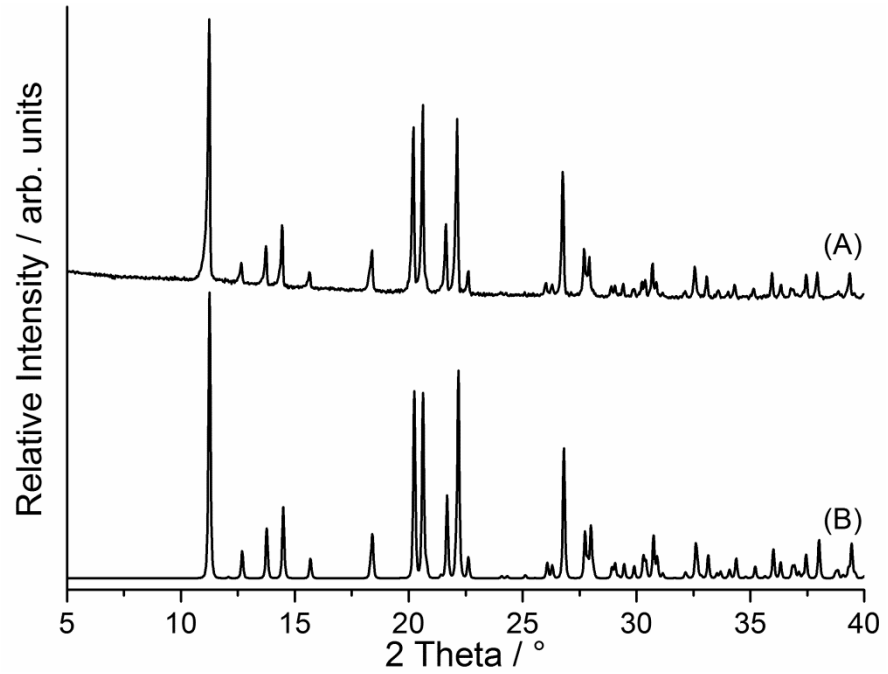

Fig. S4. Experimental XRPD pattern of **1-Fe** (A) together with the powder pattern calculated from single crystal data (B).

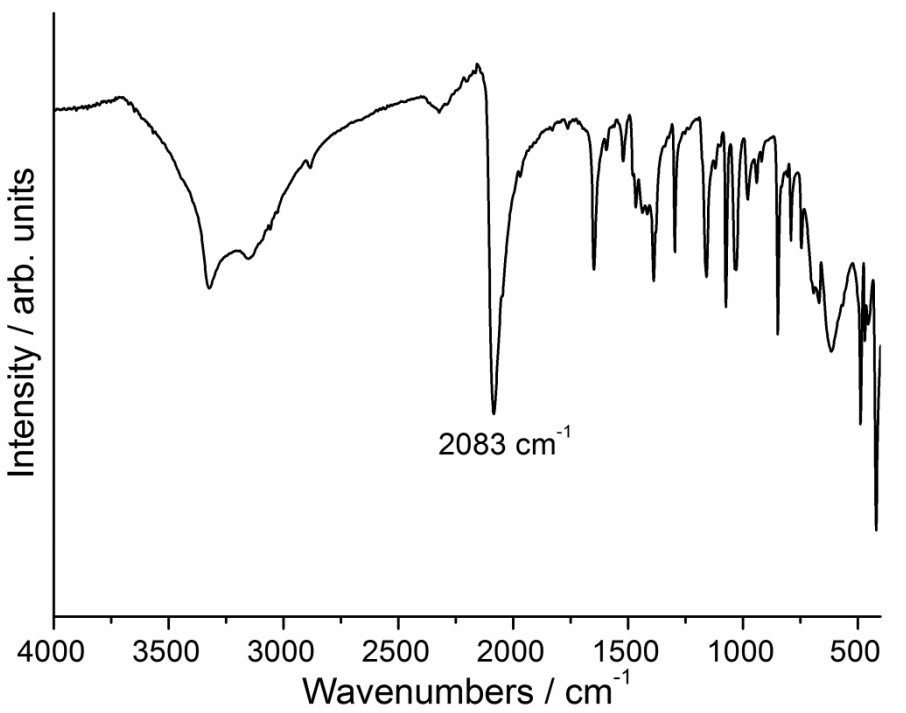

Fig. S5. IR spectrum of $Co(NCS)_2(2\text{-methylpyrazine})_2(H_2O)_2$ (**1-Co**).

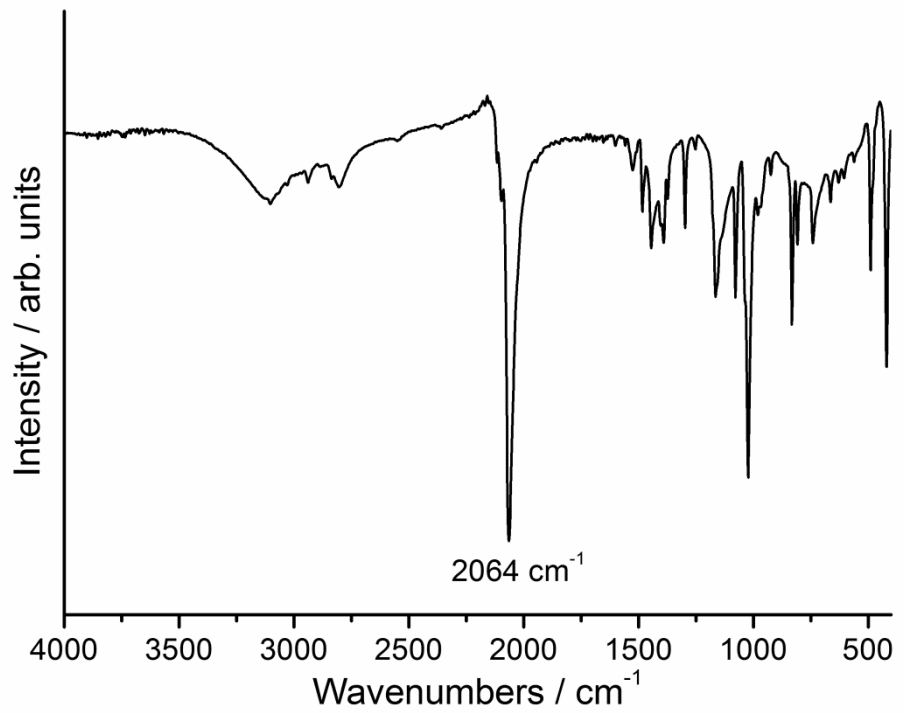

Fig. S6. IR spectrum of $Co(NCS)_2(2\text{-methylpyrazine})_2(CH_3OH)_2$ (**2-Co**).

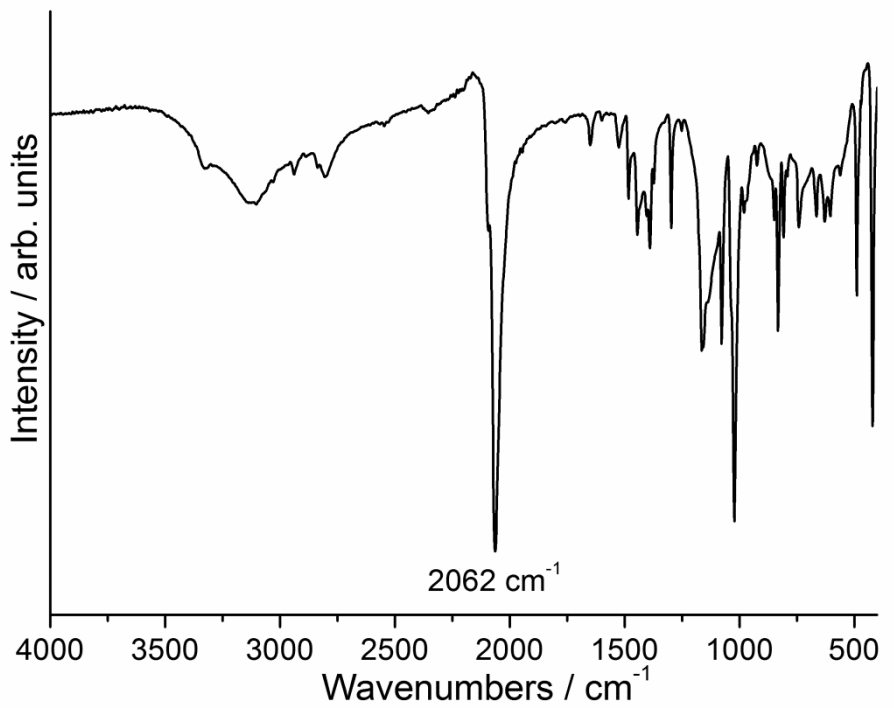

Fig. S7. IR spectrum of $Co(NCS)_2$(2-methylpyrazine)$_4$·2-methylpyrazine solvate (**3-Co**).

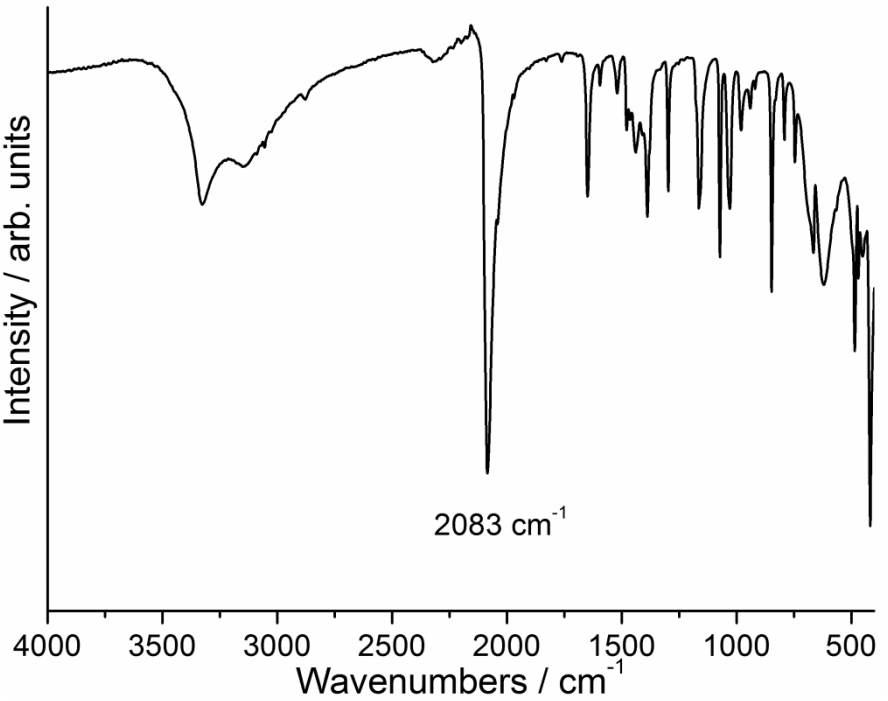

Fig. S8. IR spectrum of $Fe(NCS)_2$(2-methylpyrazine)$_2(H_2O)_2$ (**1-Fe**).

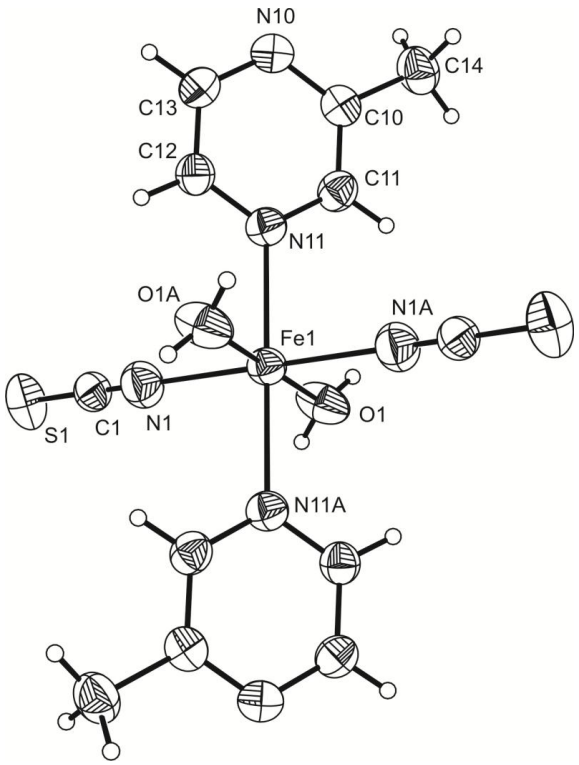

Fig. S9. ORTEP plot of $Fe(NCS)_2(2\text{-methylpyrazine})_2(H_2O)_2$ (**1-Fe**). Symmetry transformation used to generate equivalent atoms: A = -x, -y, -z + 1.

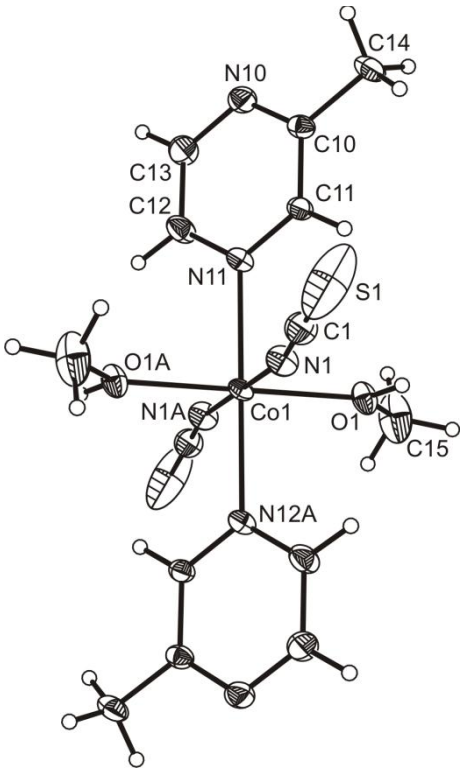

Fig. S10. ORTEP plot of $Co(NCS)_2(2\text{-methylpyrazine})_2(CH_3OH)_2$ (**2-Co**). Symmetry transformation used to generate equivalent atoms: A = -x, -y, -z + 1.

Table S1. Selected bond lengths / Å and angles / ° for $Fe(NCS)_2(2\text{-methylpyrazine})_2(H_2O)_2$ (**1-Fe**) and $Co(NCS)_2(2\text{-methylpyrazine})_2(CH_3OH)_2$ (**2-Co**). Symmetry transformation used to generate equivalent atoms: A = -x, -y, -z + 1.

	1-Fe	**2-Co**
M(1)-N(1)	2.1104(15)	2.063(3)
M(1)-N(11)	2.2205(12)	2.176(2)
M(1)-O(1)	2.1258(11)	2.103(2)
N(1A)-M(1)-N(1)	180.0	180.00(14)
N(1A)-M(1)-O(1)	91.38(6)	93.02(10)
N(1)-M(1)-O(1)	88.62(6)	86.98(10)
N(1)-M(1)-N(11)	90.46(5)	88.60(10)
N(1)-M(1)-N(11A)	89.54(5)	91.40(10)
O(1)-M(1)-O(1A)	180.0	180.0
O(1)-M(1)-N(11A)	88.90(5)	88.75(9)
O(1)-M(1)-N(11)	91.10(5)	91.25(9)

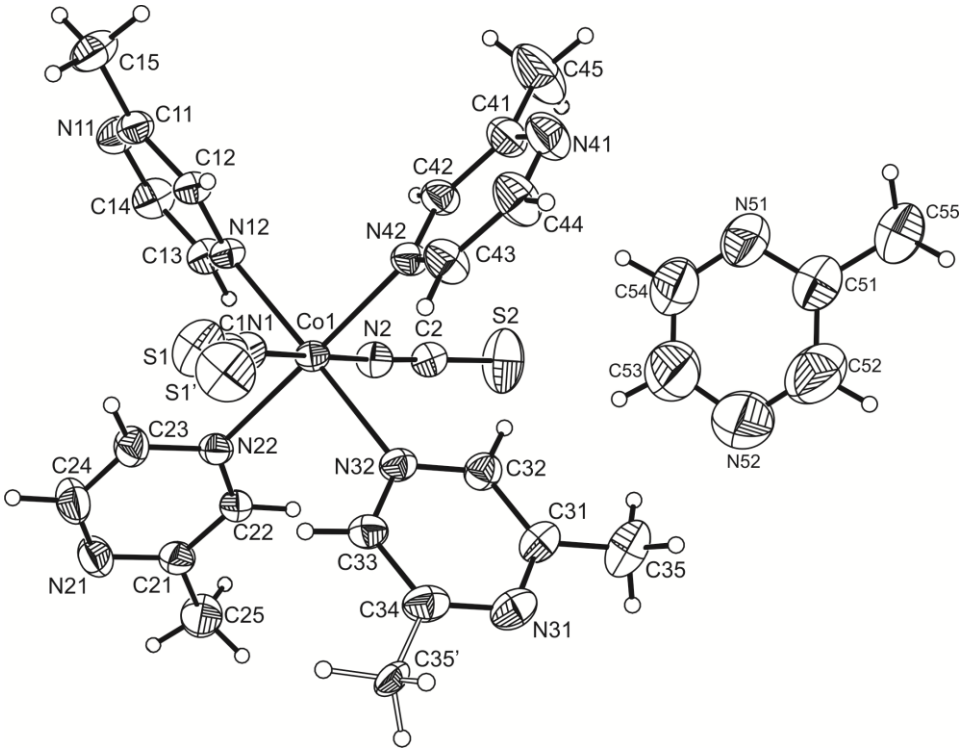

Fig. S11. ORTEP plot of $Co(NCS)_2(2\text{-methylpyrazine})_4 \cdot 2\text{-methylpyrazine}$ solvate (**3-Co**). The disordering of the non-coordinated 2-methylypyrazine ligand was omitted for clarity.

Table S2. Selected bond lengths / Å and angles / ° for $Co(NCS)_2$(2-methylpyrazine)$_4$·2-methylpyrazine solvate (**3-Co**).

compounds	**3-Co**
Co(1)-N(1)	2.063(3)
Co(1)-N(2)	2.066(2)
Co(1)-N(12)	2.191(2)
Co(1)-N(22)	2.193(2)
Co(1)-N(32)	2.186(2)
Co(1)-N(42)	2.168(2)
N(1)-Co(1)-N(2)	179.43(10)
N(1)-Co(1)-N(42)	89.79(10)
N(2)-Co(1)-N(32)	89.68(10)
N(42)-Co(1)-N(32)	89.37(9)
N(42)-Co(1)-N(12)	92.03(9)
N(32)-Co(1)-N(12)	178.57(9)
N(42)-Co(1)-N(22)	179.08(9)
N(32)-Co(1)-N(22)	91.38(9)
N(2)-Co(1)-N(42)	89.85(10)
N(1)-Co(1)-N(32)	89.88(10)
N(1)-Co(1)-N(12)	90.43(9)
N(2)-Co(1)-N(12)	90.02(9)
N(1)-Co(1)-N(22)	89.69(10)
N(2)-Co(1)-N(22)	90.67(10)
N(12)-Co(1)-N(22)	87.22(9)

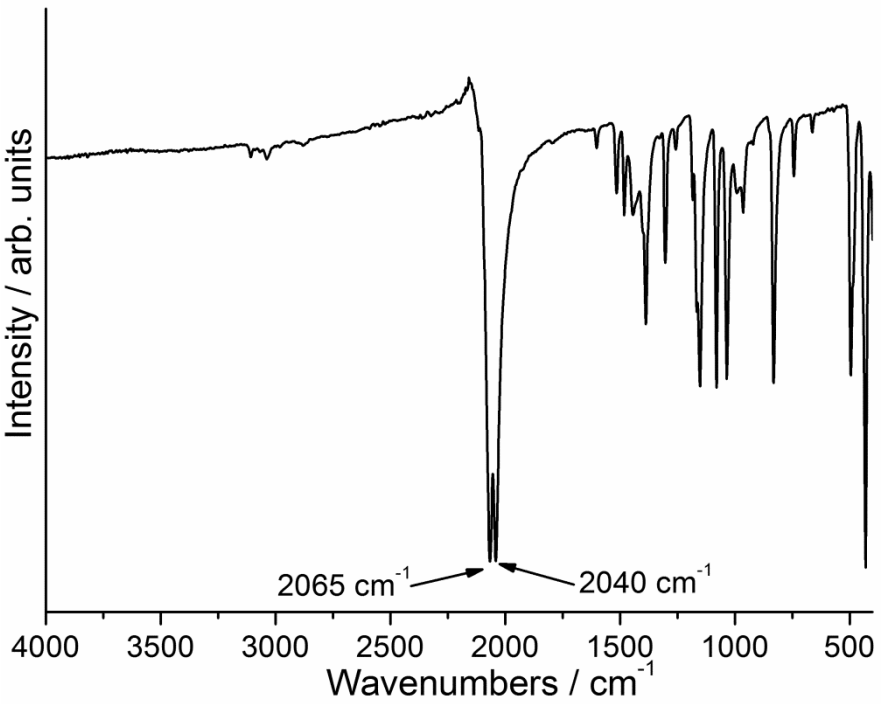

Fig. S12. IR spectrum of the residue, which was obtained in the first heating step of compound **1-Co**.

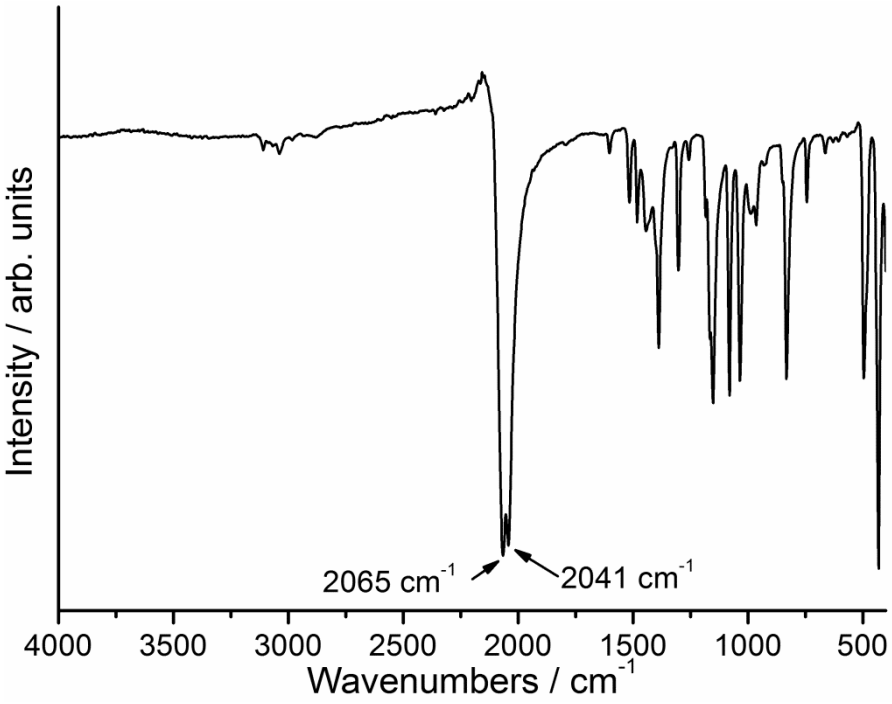

Fig. S13. IR spectrum of the residue, which was obtained in the first heating step of compound **2-Co**.

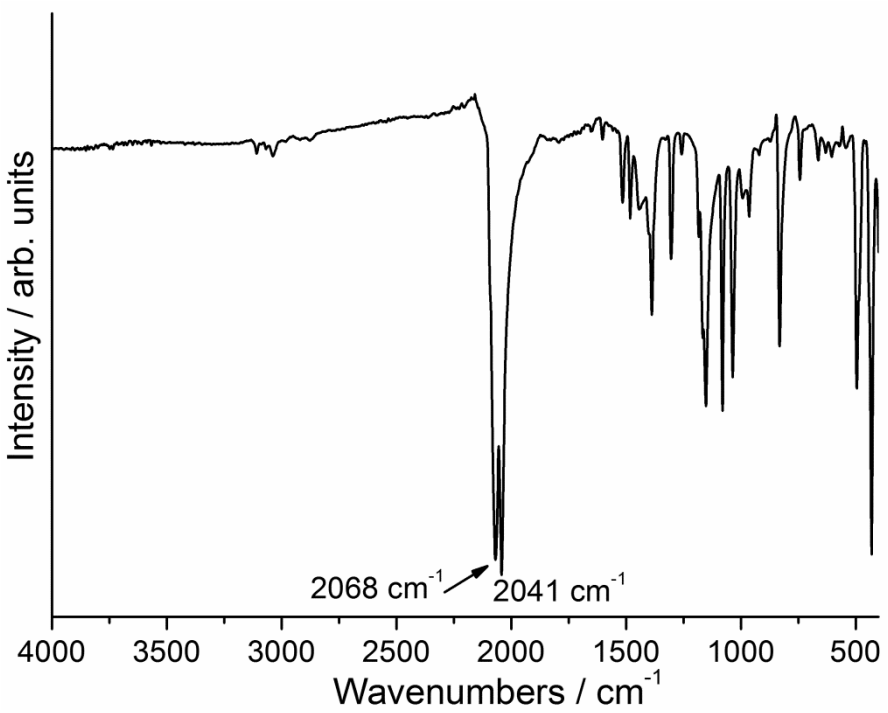

Fig. S14. IR spectrum of the residue, which was obtained in the first heating step of compound **3-Co**.

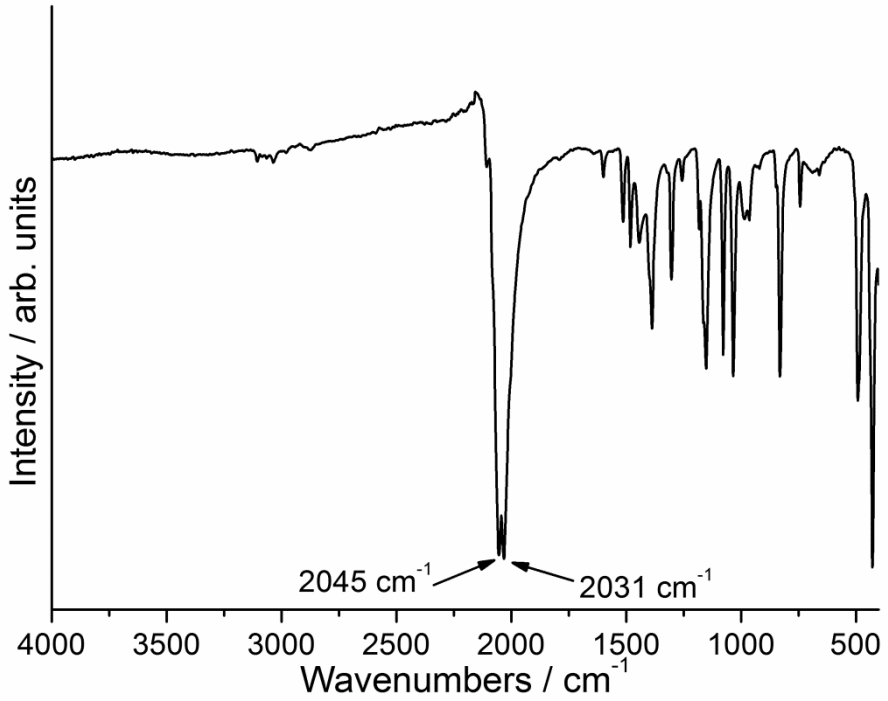

Fig. S15. IR spectrum of the residue, which was obtained in the first heating step of compound **1-Fe**.

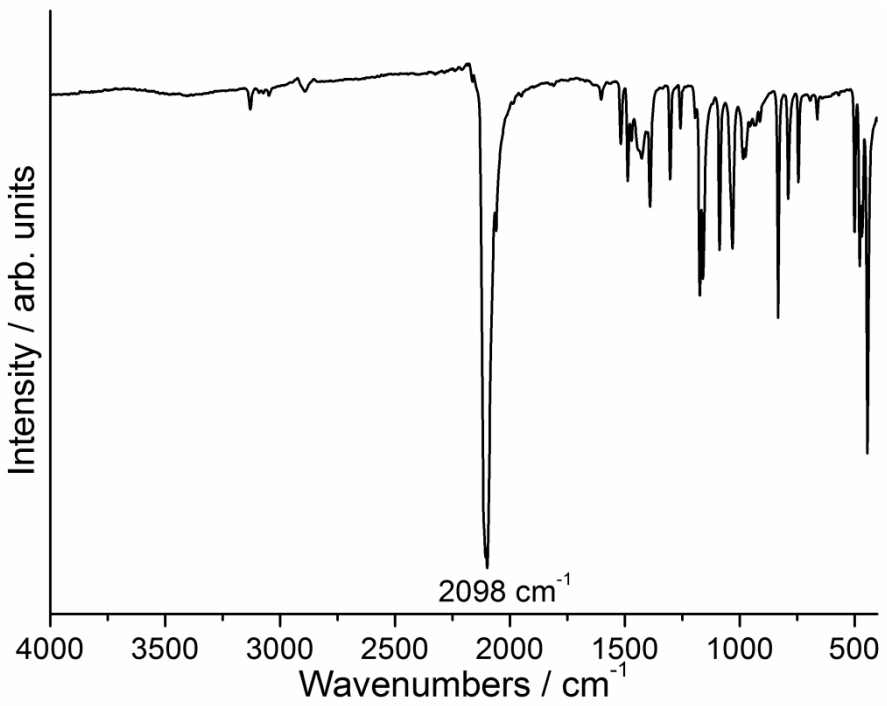

Fig. S16. IR spectrum of the residue, which was obtained in the second heating step of compound **1-Co**.

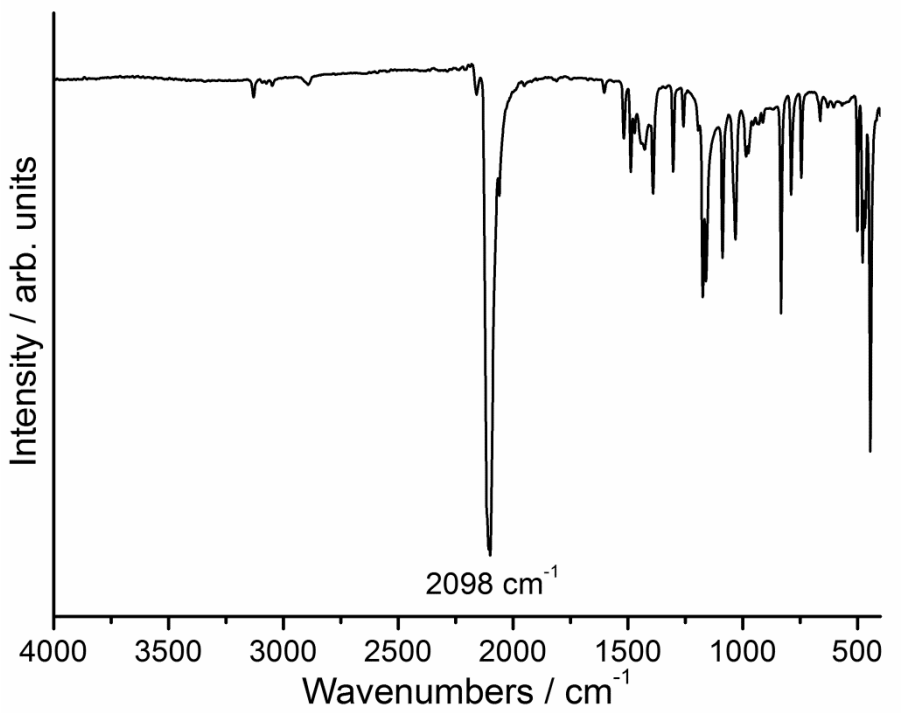

Fig. S17. IR spectrum of the residue, which was obtained in the second heating step of compound **2-Co**.

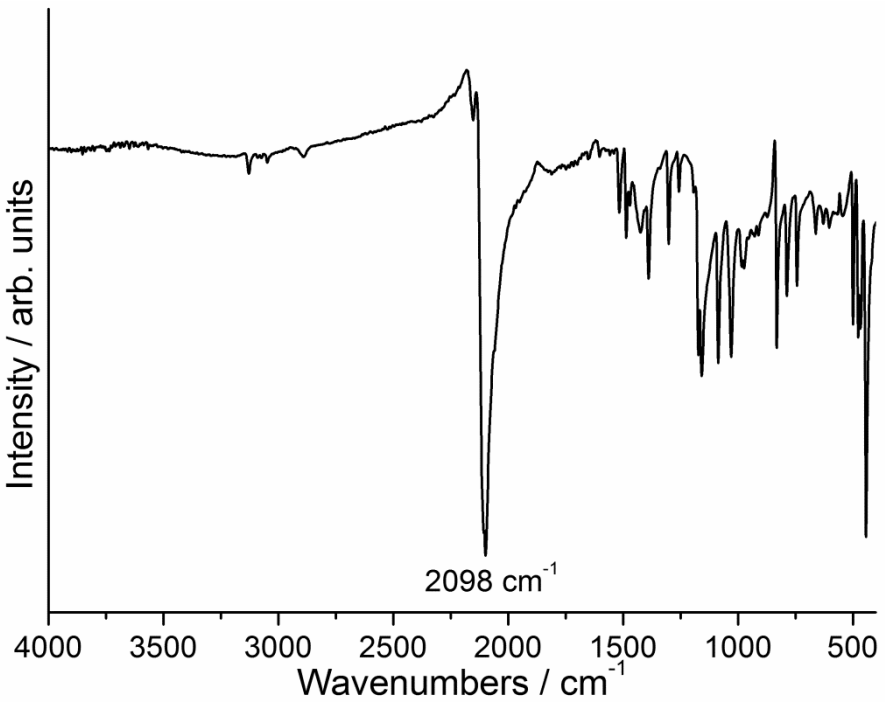

Fig. S18. IR spectrum of the residue, which was obtained in the second heating step of compound **3-Co**.

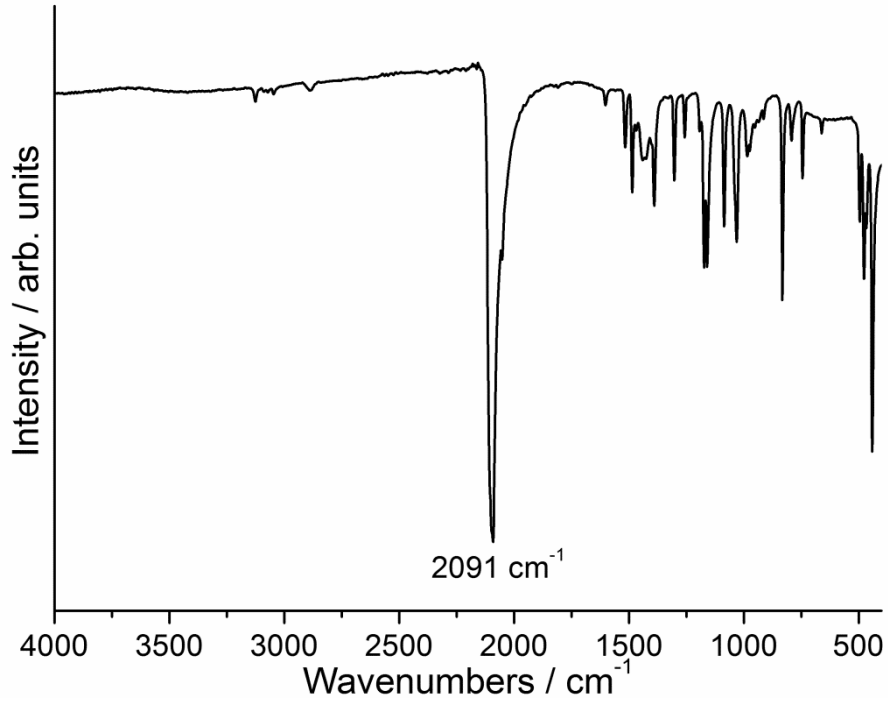

Fig. S19. IR spectrum of the residue, which was obtained in the second heating step of compound **1-Fe**.

Table S3. Selected bond lengths / Å and angles / ° for $[Cd(NCS)_2(2\text{-methylpyrazine})]_n$ (**5-Cd**). Symmetry transformation used to generate equivalent atoms: A = -x, -y + 2, -z + 1; B = -x + 1/2, y + 1/2, -z + 1/2; C = x - 1/2, -y + 3/2, z-1/2.

Cd(1)-N(1)	2.2751(19)	Cd(1)-N(11C)	2.4582(17)
Cd(1)-N(2)	2.320(2)	Cd(1)-S(1A)	2.6769(6)
Cd(1)-N(12)	2.4260(18)	Cd(1)-S(2B)	2.6842(6)
N(1)-Cd(1)-N(2)	171.84(8)	N(2)-Cd(1)-S(1A)	84.75(6)
N(1)-Cd(1)-N(12)	86.51(7)	N(12)-Cd(1)-S(1A)	91.75(5)
N(2)-Cd(1)-N(12)	85.60(7)	N(11C)-Cd(1)-S(1A)	90.64(5)
N(1)-Cd(1)-N(11C)	101.36(7)	N(1)-Cd(1)-S(2B)	93.83(5)
N(2)-Cd(1)-N(11C)	86.62(7)	N(2)-Cd(1)-S(2B)	88.03(6)
N(12)-Cd(1)-N(11C)	171.62(6)	N(12)-Cd(1)-S(2B)	88.35(5)
N(1)-Cd(1)-S(1A)	93.41(5)	N(11C)-Cd(1)-S(2B)	88.26(5)
		S(1A)-Cd(1)-S(2B)	172.753(18)

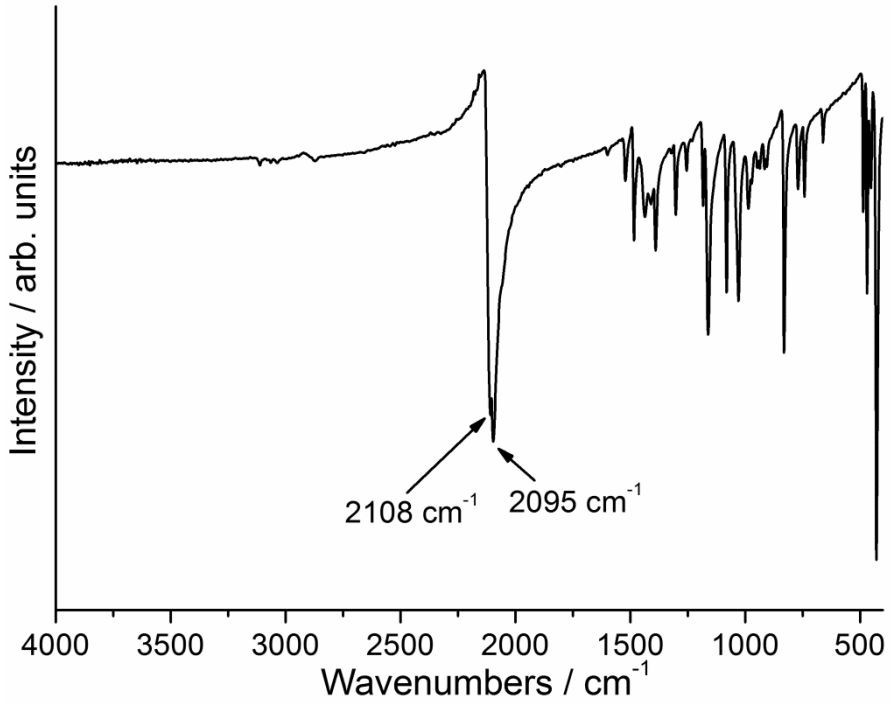

Fig. S20. IR spectrum of compound $[Cd(NCS)_2(2\text{-methylpyrazine})]_n$ (**5-Cd**).

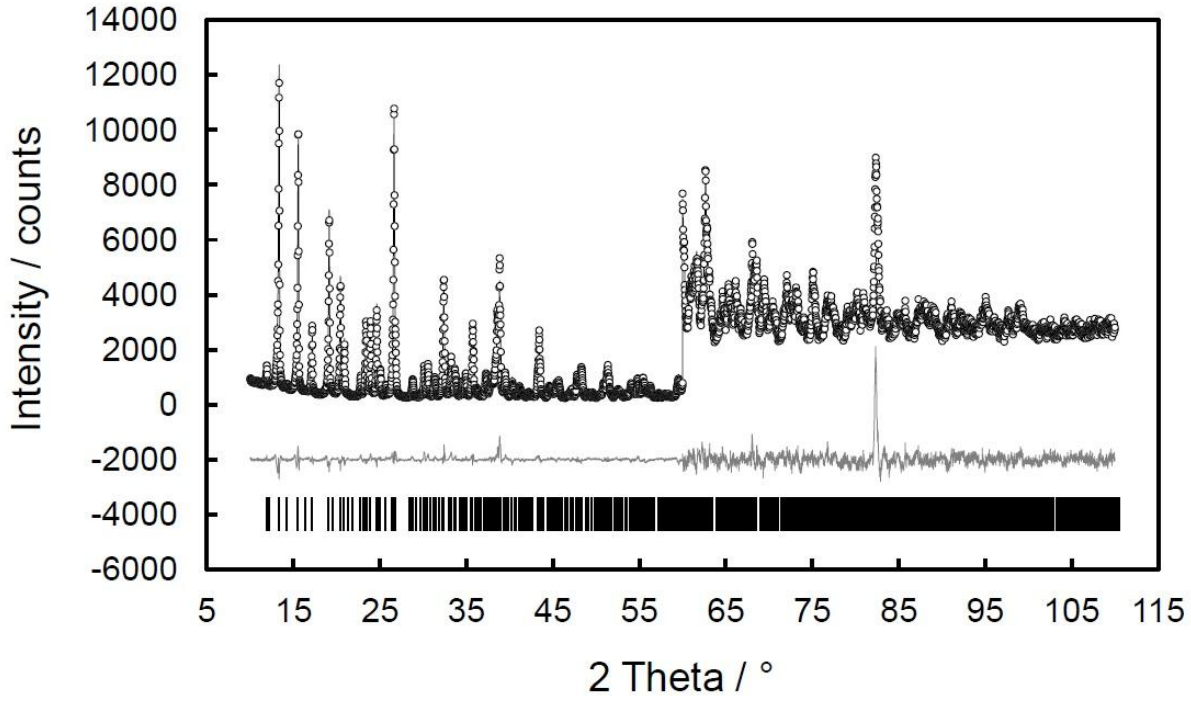

Fig. S21. Difference plot from the Rietveld refinement of $[Co(NCS)_2(2\text{-methylpyrazine})]_n$ (**5-Co**). Given are observed intensities (circles), calculated intensities (line), the difference (below, arbitrary offset for improved visibility) and the tic-marks for the reflection positions. For the second measurement (60-110° 2ϑ), intensities were scaled by a factor 5 for the sake of clarity.

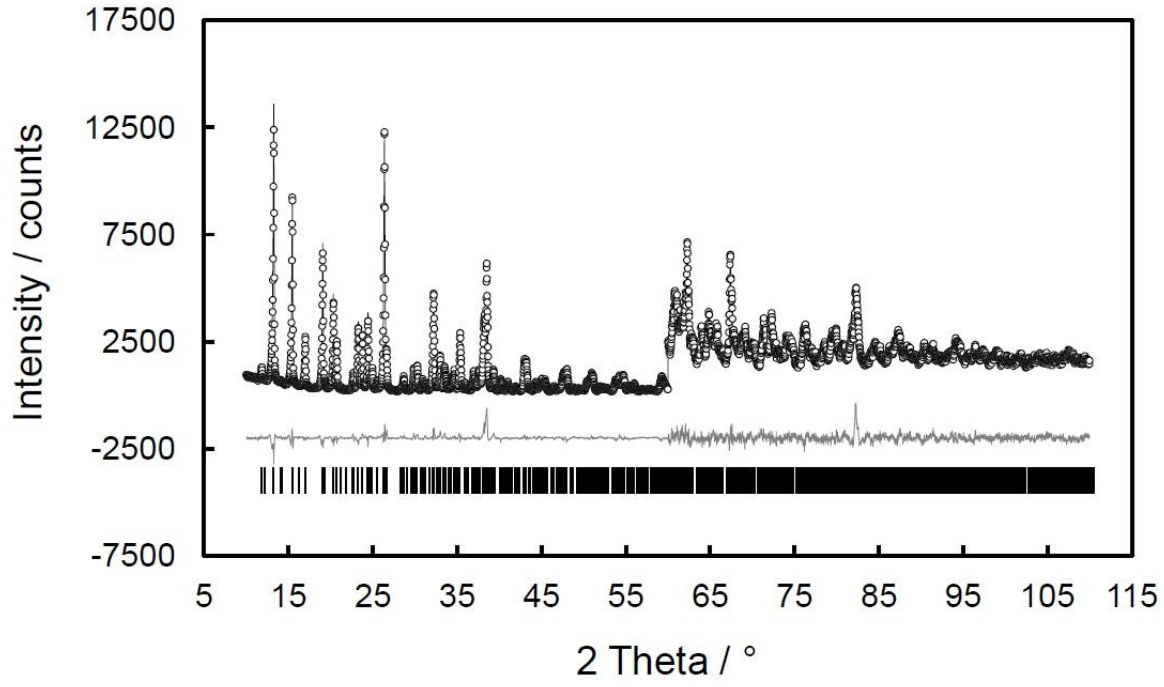

Fig. S22. Difference plot from the Rietveld refinement of $[Fe(NCS)_2(2\text{-methylpyrazine})]_n$ (**5-Fe**). Given are observed intensities (circles), calculated intensities (line), the difference (below, arbitrary offset for improved visibility) and the tic-marks for the reflection positions. For the second measurement (60-110° 2ϑ), intensities were scaled by a factor 5 for the sake of clarity.

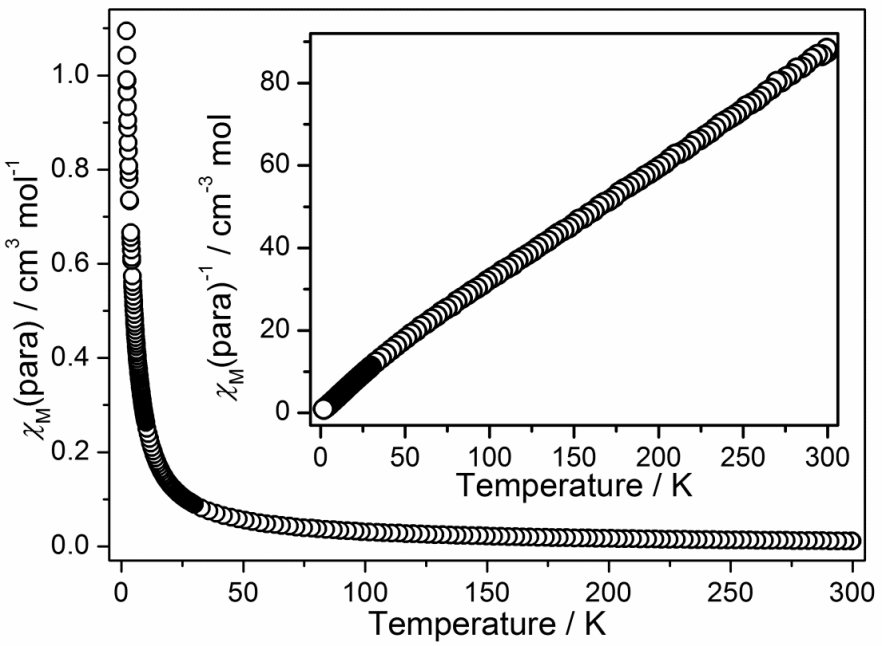

Fig. S23. Molar paramagnetic susceptibility (χ_M) and $1/\chi_M$ (inset) as function of temperature at H_{DC} = 1 kOe for **4-Co**.

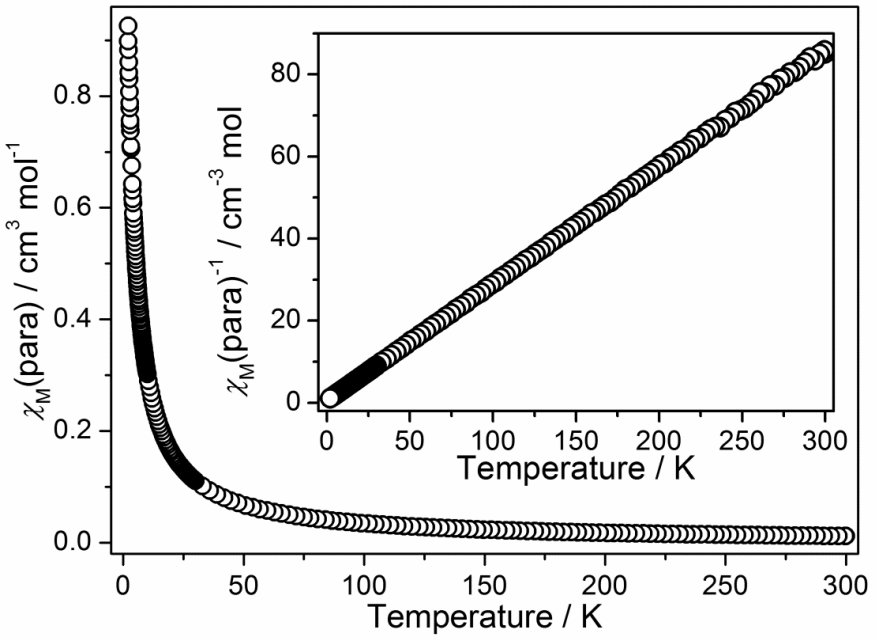

Fig. S24. Molar paramagnetic susceptibility (χ_M) and $1/\chi_M$ (inset) as function of temperature at H_{DC} = 1 kOe for **4-Fe**.

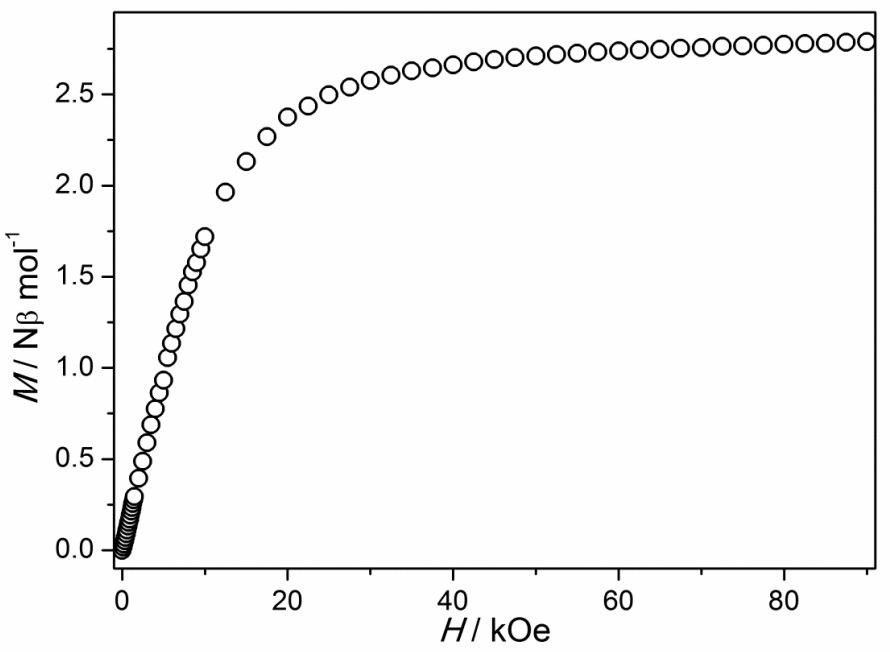

Fig. S25. Initial curve in range of 0 – 90 kOe at T = 2 K for **4-Co**.

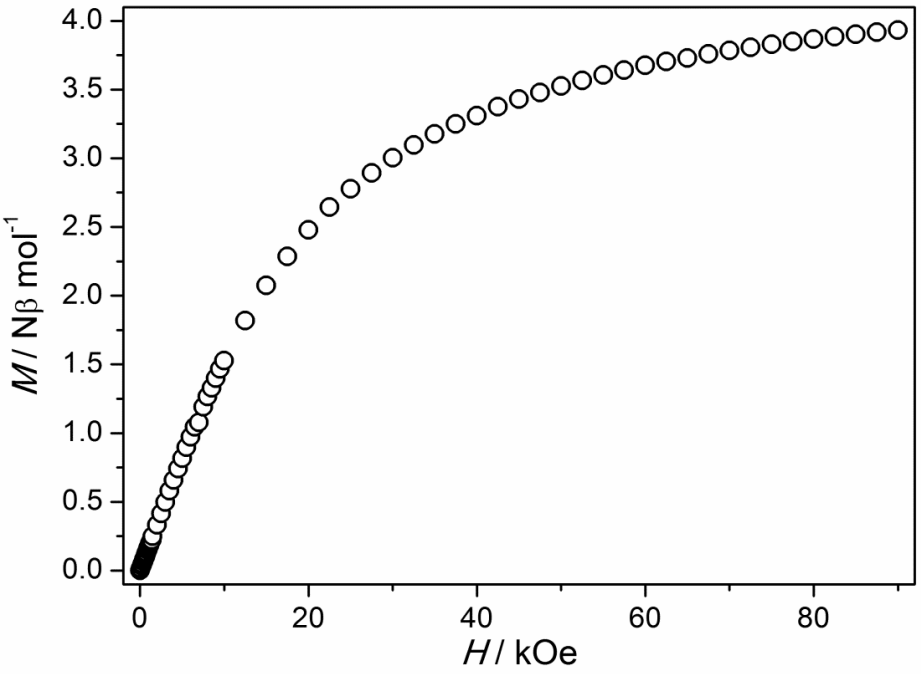

Fig. S26. Initial curve in range of 0 – 90 kOe at T = 2 K for **4-Fe**.

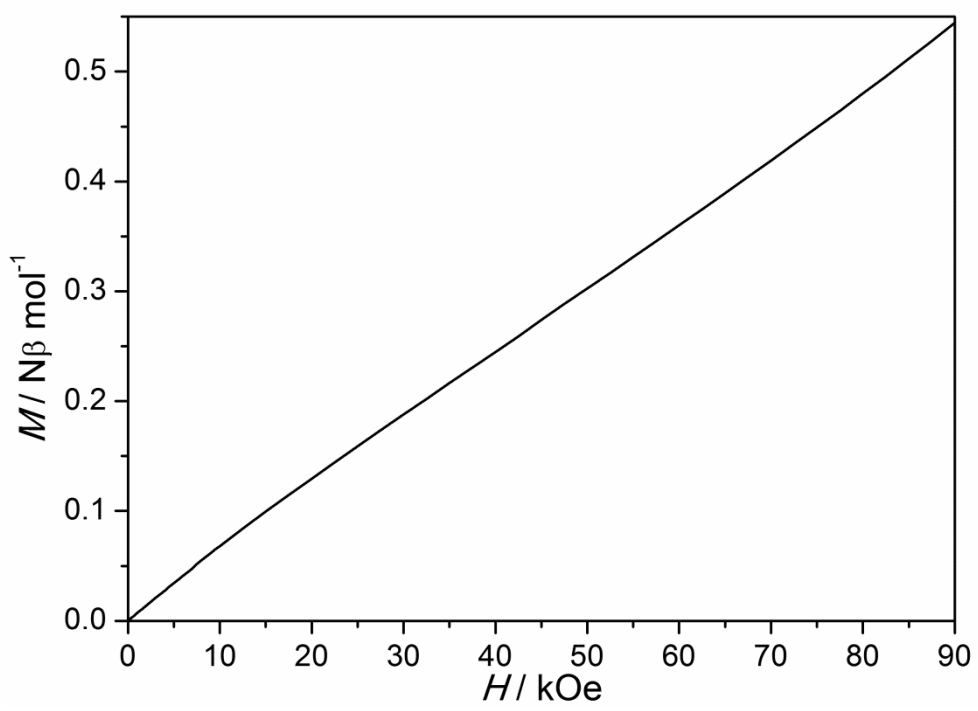

Fig. S27. Initial curve in range of 0 – 90 kOe at T = 2 K for **5-Fe**.

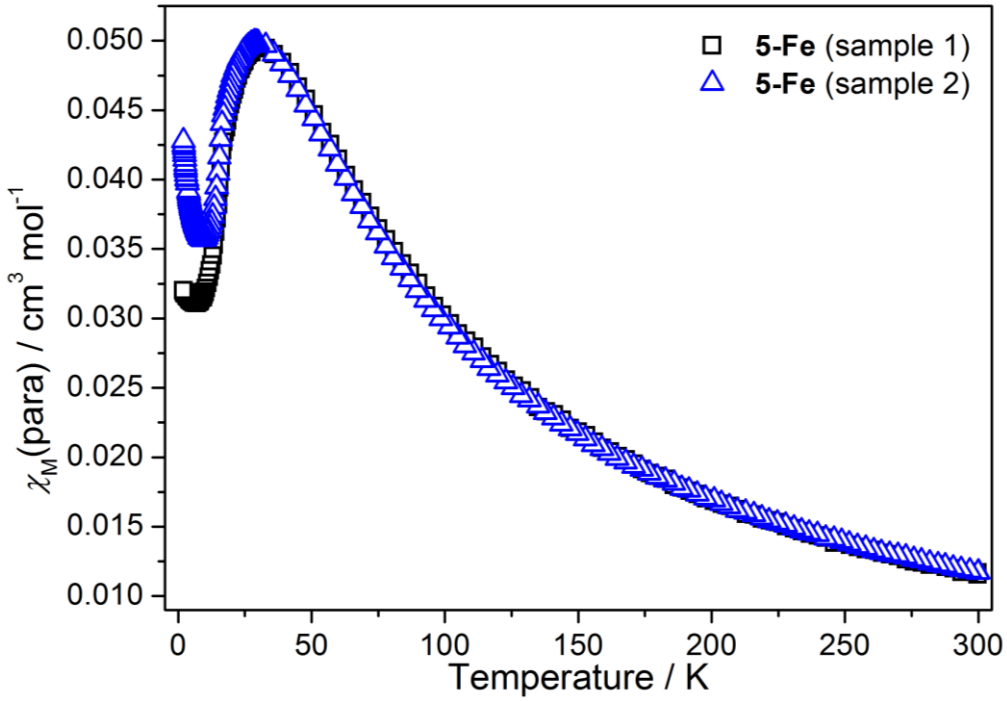

Fig. S28. Molar paramagnetic susceptibility (χ_M) as function of temperature at H_{DC} = 1 kOe for two different batches of **5-Fe**.

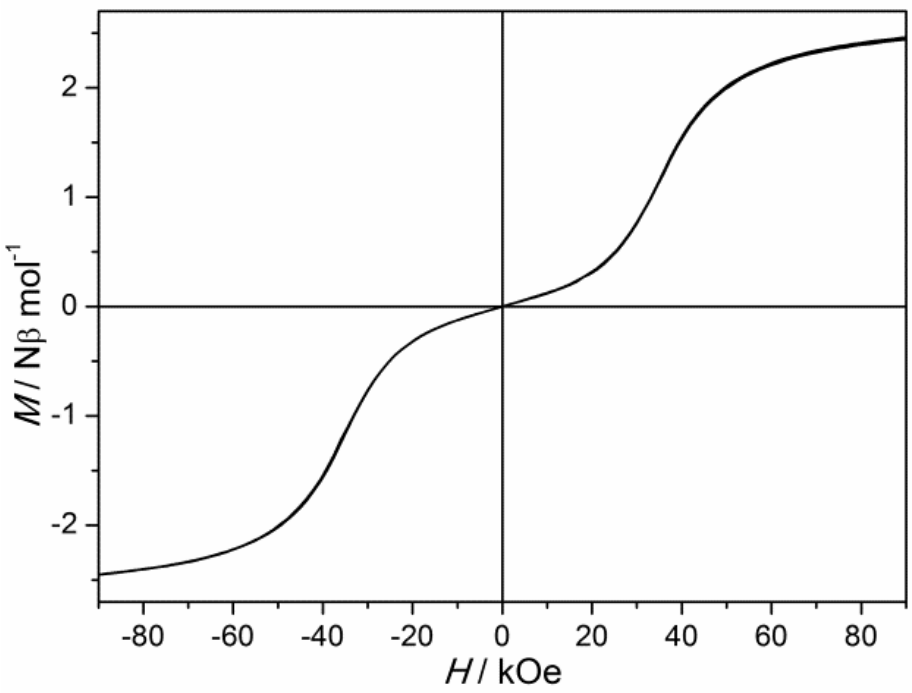

Fig. S29. Saturation magnetization experiment at T = 2 K in range of ±90 kOe for **5-Co**.

Table S4. Results of the magnetic measurements at H_{DC} = 40-90 kOe for **5-Co**.

H_{DC} / kOe	40	50	60	70	80	90
C / $cm^3K \cdot mol^{-1}$	3.54	3.56	3.58	3.58	3.58	3.57
θ / K	-20.5	-20.6	-21.2	-21.4	-21.7	-22.2
μ_{eff}(exp) / μ_B	5.32	5.34	5.35	5.35	5.35	5.35
μ_{eff}(exp) / μ_B			3.87			

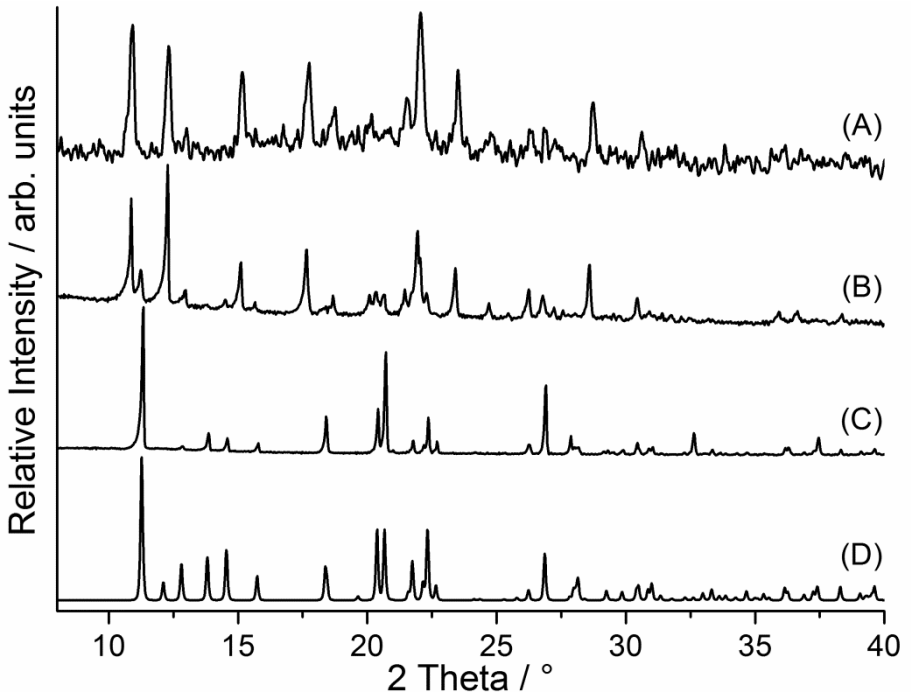

Fig. S30. Experimental XRPD of **2-Co** (A) which were stored for 15 min. (B) and for 1 d in a humid atmosphere (C) together with the calculated powder pattern for **1-Co** (D).